Research Article

Modelling and comparative analysis of ANN and PID controllers with MFB applied to HESS of electric vehicle

Raghavaiah Katuri[1] · Srinivasarao Gorantla[1]

Abstract

A control strategy approach is proposed, in order to achieve the smooth and precise switching of energy sources present in the hybrid energy storage system which includes battery and ultracapacitor. Based on the speed of an electric motor four individual math functions are considered, designed a new controller named as math function-based (MFB) controller. Thereafter the designed MFB controller is integrated with conventional/intelligent controller to full fill the proposed control strategy approach. Two different hybrid controllers MFB with proportional integral derivative, MFB with artificial neural network are proposed and implemented to the electric motor in four different modes based on the load applied. Two-hybrid controllers MATLAB/Simulink output responses are compared and tabulated in the conclusion section.

Keywords BDC · UDC · PID controller · ANN controller · Battery · UC · MFB controller · Electric vehicle

1 Introduction

Two real-time controllers are realized for proper current sharing in an optimal way in between batteries and UCs. The first controller is realized with the help of Karush–Kuhn–Tucker conditions an optimized problem is formulated which are used to construct the controller for the better splitting of the current related to the load requirement. The second one is realized as an intelligent controller and is attained from the neural network. The battery state of health (SOH) is considered in order to find the relative performance of both the real-time controllers this phenomenon mainly tells about the difference between two controllers. A real-time hardware prototype experimental setup was built with HESS for practical validation. Both controllers' simulation as well as hardware realization is done and compared the two controller's performance to the better controller for the splitting of current between energy sources [1–3].

One variable rate-limit function is considered to attain the adoptive rate limit controller for HESS. The intended control technique provides the protection to the main power source against sudden load changes by drawing sudden power from the supporting source. The designed controller saves the life of the main power source by reducing the stress on that which means the main power source can feed the load during normal load condition [4–6].

A new HESS is proposed with two different character power source including with feasible control technique. The considered control technique is mainly reducing, the surges appear during changing of the sources one to another. Here one BDC is considered for the forward and backward flow of power in the circuit. In this two-source battery, UC connected to BDC in the circuit. The complete circuit model is subdivided into four cases, to attain better knowledge about the considered HESS with controller action. The BDC is operated satisfactorily within the range of power limits [7, 8].

In this, a novel HESS is introduced for better acceleration and driving range of the vehicle. The Conventional HESS sourced vehicles require a high rating of DC–DC converters for the successful operation of the vehicle during

all road conditions. With this arrangement, a relatively constant voltage profile is created which enhances the lifetime of the battery [9, 10].

2 System with proposed control strategy

The proposed control technique mainly includes two energy sources, two converters, and different controllers. The bidirectional converter (BDC) will perform the buck and boost operation on the other hand unidirectional (UDC) performs only boost operation. The battery present in the work is acting as a base source on the other hand UC will treat as a supporting source. Total three switches S1, S2 and S3 are combined present in the two converters in which switch two, three are related to BDC a switch one is present in UDC. Two different controllers are used in which MFB is a newly designed one and the other one is the conventional one which is used to develop the controlled pulse signals to the converters (Fig. 1).

Figure 2 represents that the DC–DC converter model implemented with the main circuit for EV application.
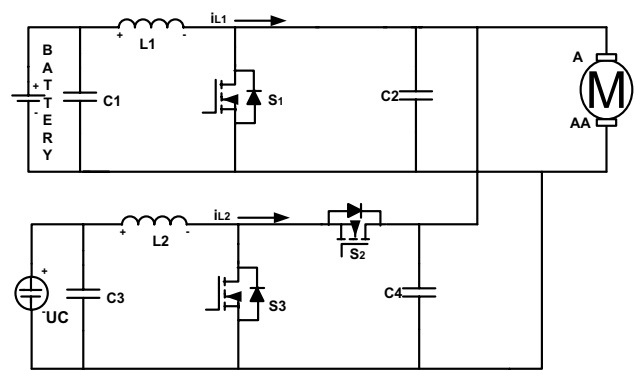
Fig. 2 DC–DC converter representation with an electric motor

which can be represented with Fig. 3. During case two, both the source will share the energy and give it to the load, Fig. 4 reflecting this mode of operation. In case three only base source will send the required power to the load, which shows in Fig. 5. And the last case of operation both converters are in operation, one is for supplying power and one power recharge the UC, which is clear from Fig. 6.

3 Four different cases with proposed control strategy

The power splitting between two energy sources has been analysed with four different cases which are corresponding to the applied torque on the motor. In first case-controlled pulse signals are developed to only BDC (boost) and no controlled signal are developed to UDC

4 Generalized model of DC–DC converters used in proposed technique

In this work, providing a controlled signal to the switch of UDC or BDC is plays a vital role during the transition of energy source [11]. So, it is necessary to know the functioning of converters during the ON/OFF state, which can be obtained and discussed in this section in detail.

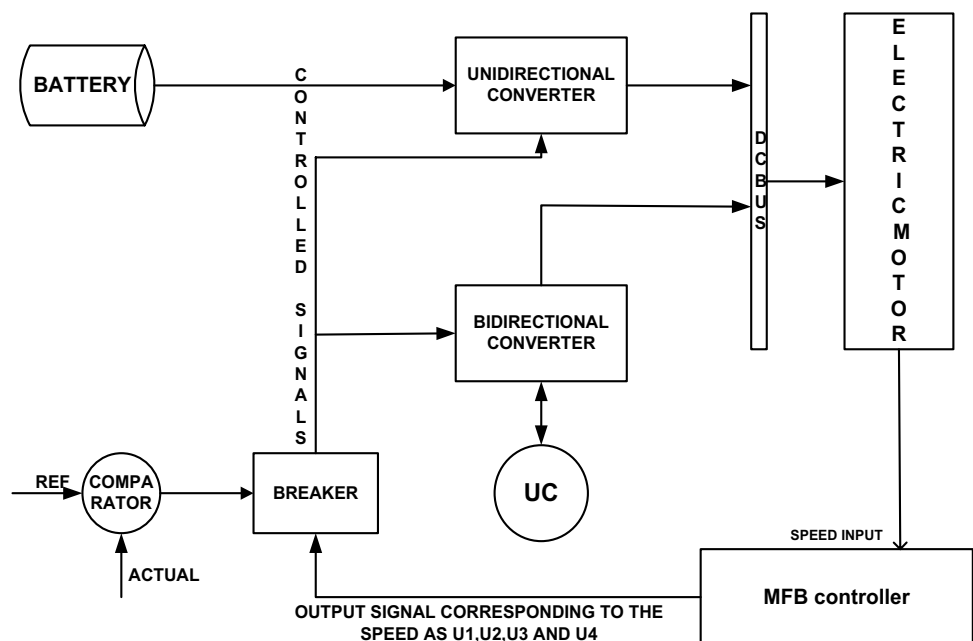**Fig. 1** Block diagram with the proposed control strategy

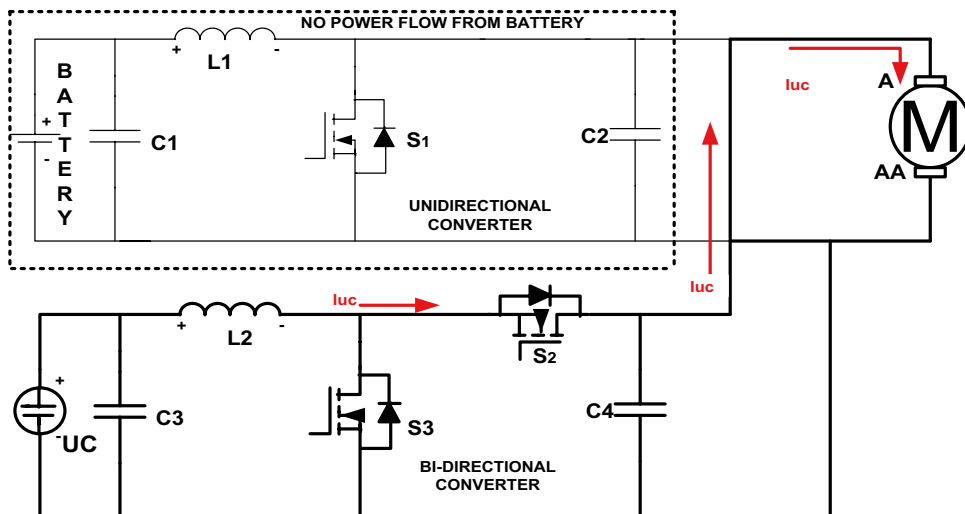**Fig. 3** DC–DC converter representation with electric motor during case-1 operation

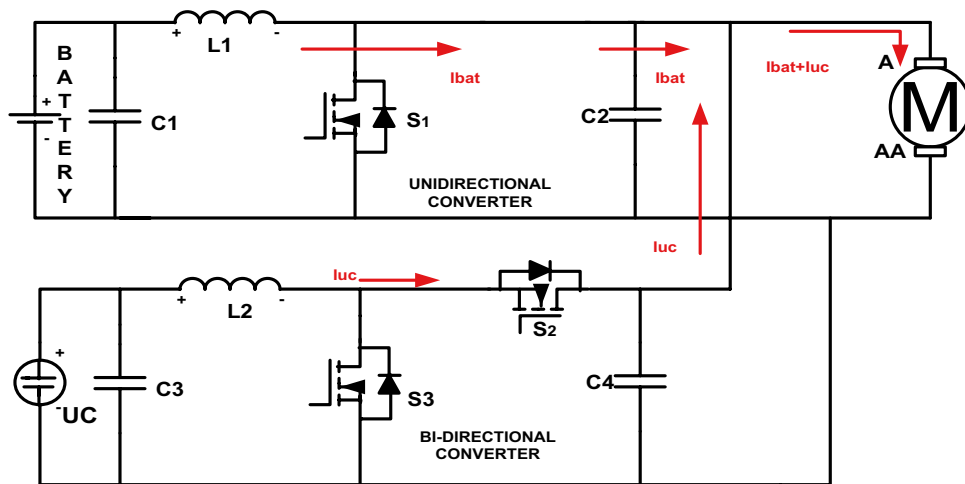**Fig. 4** DC–DC converter representation with electric motor during case-2 operation

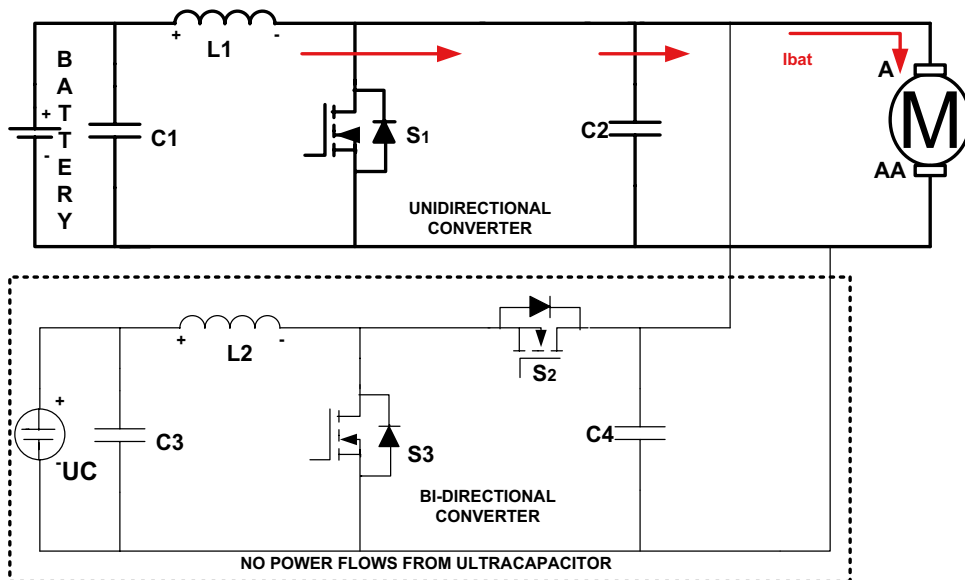**Fig. 5** DC–DC converter representation with electric motor during case-3 operation

Fig. 6 DC–DC converter representation with electric motor during case-4 operation
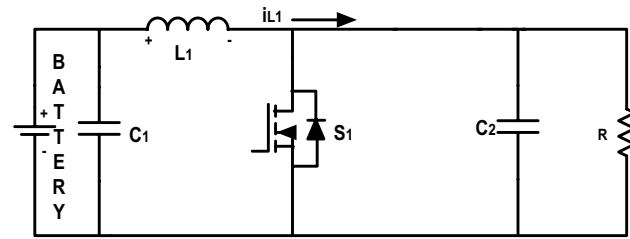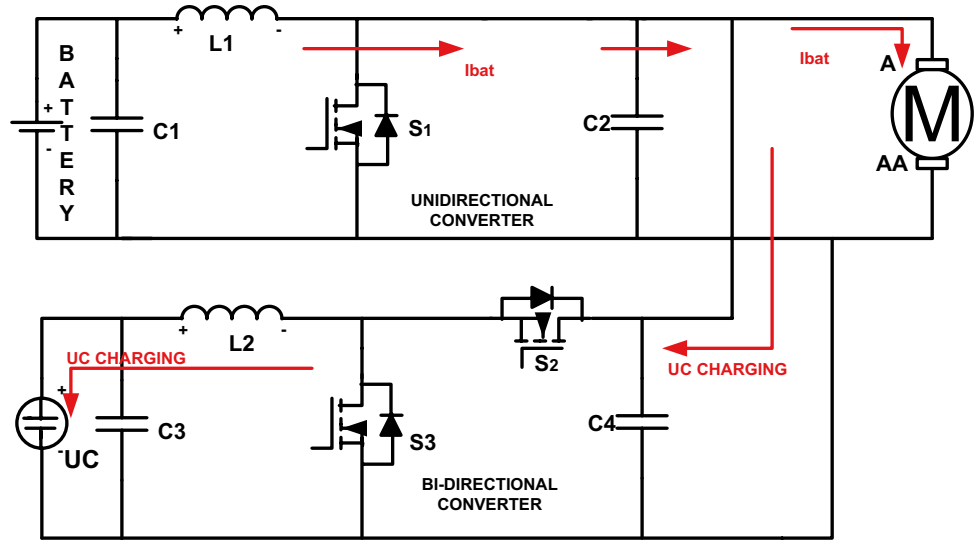

Fig. 7 DC–DC unidirectional converter representation

4.1 Unidirectional converter

The voltage across inductor present in UDC is given by (Fig. 7)

$$V = L\frac{di}{dt} \tag{1}$$

$$i = \frac{1}{L}\int_0^t V dt + i_0 \tag{2}$$

If the switch is in ON condition

$$i_{pk} = \frac{(V_0 - V_i)T_{on}}{L} \tag{3}$$

$$\Delta i = \frac{(V_0 - VT_{mos})T_{on}}{L} \tag{4}$$

If the switch is in OFF condition

$$i_{pk} = i_0 = \frac{(V_0 - V_i + V_D)T_{off}}{L} \tag{5}$$

$$\Delta i = \frac{(V_0 - V_i + V_D)T_{off}}{L} \tag{6}$$

If Vmos is the voltage across MOSFET and V_D is the voltage across the diode, the output voltage equation becomes

$$V_0 = \frac{(V_0 - Vmos) * \delta}{L} - V_D \tag{7}$$

After neglecting diode voltage and MOSFET voltage the final voltage becomes

$$V_0 = \frac{V_i}{1 - \delta} \tag{8}$$

4.2 Bidirectional converter

In order to obtain the proper switching between battery and UC according to the vehicle dynamics, one BDC is required. The current flows direction may be in any direction that may be forward to back or backward to forward, which is decided by the mode of operation of the BDC that may be boost or buck mode. The power will flow from high voltage to low voltage during boost operation on the other hand vice versa happens during buck mode of operation (Fig. 8).

Boost mode operation:

$$\delta = \frac{t_{on}}{t_{on} + t_{off}} = \frac{t_{on}}{T} \tag{9}$$

During boost mode, itself the switch present in BDC will alter in order to boost the voltage level depending upon the requirement. So, during boost mode itself, the
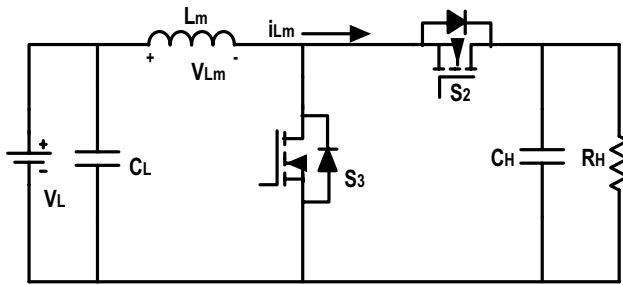
Fig. 8 DC–DC bidirectional converter representation

switches action can be analysed by splitting the period in association with the duty cycle.

If the switch is in closed $S_1 (0 \le t < \delta T)$:

In this position, switch S1 in ON state and S2 in OFF state, which causes the low voltage side source, and inductor both are in parallel combination. In addition, the equation related to this action is given as

$$v_{Lm} = V_L = L_m \frac{di_{Lm}}{dt} \tag{10}$$

The rate of change of inductor current is given as

$$\frac{\Delta i_{Lm}}{\Delta t} = \frac{\Delta i_{Lm}}{\delta T} = \frac{V_L}{L_m} \tag{11}$$

Above equations can be rewritten as (Fig. 9)

$$\Delta i_{Lm(on-time)} = \frac{V_L}{L_m} \delta T \tag{12}$$

If the switch is in open position $S_1 (\delta T \le t < T)$:

The switch at low voltage side is opened and high voltage side switch is in ON state, which makes that the source voltage and inductor voltage together as a series combination. The voltage across induction can be written as

$$v_{Lm} = V_L - V_H = L_m \frac{di_{Lm}}{dt} \tag{13}$$

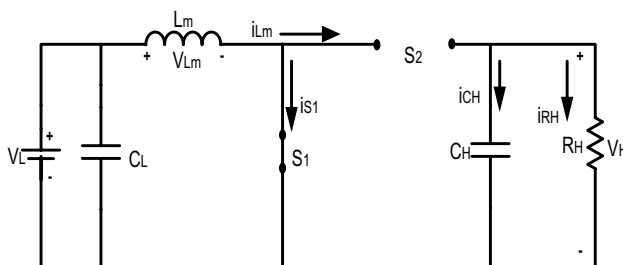After simplification above equation can be written as

$$\frac{di_{Lm}}{dt} = \frac{V_L - V_H}{L_m} \tag{14}$$

Due to the OFF condition of S1 the state of inductor current can be written as

$$\frac{\Delta i_{Lm}}{\Delta t} = \frac{\Delta i_{Lm}}{(1-\delta)T} = \frac{V_L - V_H}{L_m} \tag{15}$$

And the above equation can be rewritten as

$$\Delta i_{Lm(off-time)} = \frac{V_L - V_H}{L_m}(1-\delta)T \tag{16}$$

Under stable state condition, the change in inductor current in a single cycle can be expressed as

$$\Delta i_{Lm(on-time)} + \Delta i_{Lm(off-time)} = 0 \tag{17}$$

After inserting original equations of change in inductor current, the above equations become

$$\frac{V_L}{L_m}\delta T + \frac{V_L - V_H}{L_m}(1-\delta)T = 0 \tag{18}$$

After simplification above equation can be written as

$$V_L \delta + (V_L - V_H)(1-\delta) = 0 \tag{19}$$

The high and low voltage side relation can represent as

$$V_H = \frac{1}{1-\delta}V_L \tag{20}$$

From the above relation, the duty cycle value varies between $0 \le \delta \le 1$ and the output of the BDC is always greater than the input (Fig. 10).

Design of capacitor value:

The capacitor connected at high voltage side is capable to maintain high voltage during boost mode condition during the steady-state condition. But the high voltage value will change due to dynamics of the load, the variable charge of the capacitor can be expressed as

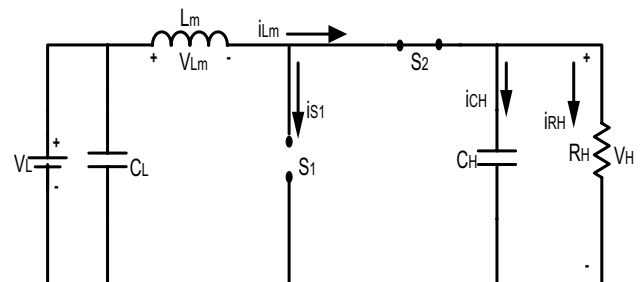$$|\Delta Q_H| = \frac{V_H}{R_H}\delta T = C_H \Delta V_H \tag{21}$$

Fig. 9 DC–DC bidirectional converter representation under boost mode, switch S2 ON condition

Fig. 10 DC–DC bidirectional converter representation under boost mode, switch S2 ON condition

In addition, the ripple voltage can be expressed as

$$\Delta V_H = \frac{V_H \delta T}{R_H C_H} = \frac{V_H \delta}{R_H C_H f} \tag{22}$$

Rewritten as

$$C_H = \frac{\delta}{R_H f \left(\Delta V_H / V_H \right)} \tag{23}$$

Inductor design:
After neglecting all line losses, the low voltage side power can be equivalent to that the high voltage side power value as follows

$$V_L I_{Lm} = \frac{V_H^2}{R_H} = \frac{\left(V_L / (1 - \delta) \right)^2}{R_H} = \frac{V_L^2}{(1-\delta)^2 R_H} \tag{24}$$

The mean value of the inductor current can be written as

$$I_{Lm} = \frac{V_L^2}{(1-\delta)^2 R_H} \tag{25}$$

The maximum and minimum values of the inductor current can be obtained by

$$I_{Lm}\_max = I_{Lm} + \frac{\Delta i_{Lm}}{2} = \frac{V_L}{(1-\delta)^2 R_H} + \frac{V_L}{2L_m}\delta T \tag{26}$$

$$I_{Lm}\_min = I_{Lm} - \frac{\Delta i_{Lm}}{2} = \frac{V_L}{(1-\delta)^2 R_H} - \frac{V_L}{2L_m}\delta T \tag{27}$$

Under continuous current mode condition, the inductor current should always greater than zero

$$\frac{V_L}{(1-\delta)^2 R_H} - \frac{V_L}{2L_m}\delta T \geq 0 \tag{28}$$

During continuous current mode, the minimum inductor current should be

$$L_m,min \geq \frac{\delta(1-\delta)^2 R_H}{2f} \tag{29}$$

Buck mode operation:
This section describes the BDC operation under buck mode and revelling the design procedure of the components present in the circuit
If the switch is in closed condition $S_2(0 \leq t < \delta T)$:
Now the switch S2 is appearing at high voltage side and the inductor voltage appearing at both ends is given as

$$v_{Lm} = V_H - V_L = L_m \frac{di_{Lm}}{dt} \tag{30}$$

The simplified equation can be written as

$$\frac{di_{Lm}}{dt} = \frac{V_L - V_H}{L_m} \tag{31}$$

When the switch is closed then the change of inductor current is

$$\frac{\Delta i_{Lm}}{\Delta t} = \frac{\Delta i_{Lm}}{\delta T} = \frac{V_H - V_L}{L_m} \tag{32}$$

Above equation can be written as (Fig. 11)

$$\Delta i_{Lm(on-time)} = \frac{V_H - V_L}{L_m}\delta T \tag{33}$$

If the switch is in open condition $S_2(\delta T \leq t < T)$:
The voltage value of both ends of BDC is

$$v_{Lm} = -V_L = L_m \frac{di_{Lm}}{dt} \tag{34}$$

The simplified equation can be written as

$$\frac{di_{Lm}}{dt} = \frac{-V}{L_m} \tag{35}$$

The rate of change of current value is

$$\frac{\Delta i_{Lm}}{\Delta t} = \frac{\Delta i_{Lm}}{(1-\delta)T} = -\frac{V_L}{L_m} \tag{36}$$

Simplified equation is

$$\Delta i_{Lm(off-time)} = -\frac{V_L}{L_m}(1-\delta)T \tag{37}$$

Under the steady-state condition, the total change of inductor current should be zero

$$\Delta i_{Lm(on-time)} + \Delta i_{Lm(off-time)} = 0 \tag{38}$$

After substituting all values above, the equation becomes

$$\frac{V_H - V_L}{L_m}\delta T - \frac{V_L}{L_m}(1-\delta)T = 0 \tag{39}$$

Simplified equations as

$$(V_H - V_L)\delta T - V_L(1-\delta)T = 0 \tag{40}$$
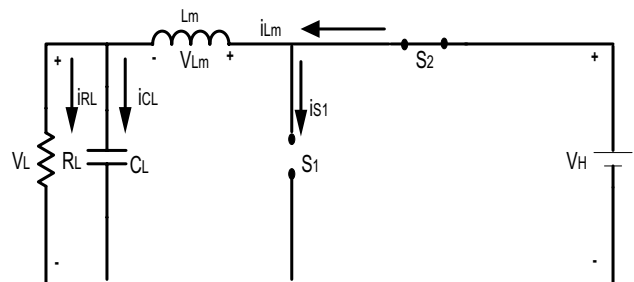

Fig. 11 DC–DC bidirectional converter representation under buck mode, switch S2 ON condition

The low and high voltage relationship of this mode of operation can be expressed as

$$V_L = V_H \delta \qquad (41)$$

During this mode of operation, the voltage at the input is lesser than that output side and the duty cycle value always $0 \leq \delta \leq 1$(Fig. 12).

Design of Capacitor:

The current flows in the low voltage side capacitor are

$$i_{CL} = i_{Lm} - i_{RL} \qquad (42)$$

Rate of change of the capacitor charges is given as

$$\Delta Q_L = C_L \Delta V_L \qquad (43)$$

After calculating, the positive area current equation can be written as

$$\Delta Q_L = \frac{T \Delta i_{Lm}}{8} \qquad (44)$$

The ripple content in the low voltage side can be found from

$$\Delta V_L = \frac{T \Delta i_{Lm}}{8 C_L} \qquad (45)$$

After replacing some values above equation becomes

$$\Delta V_L = \frac{V_L(1 - \delta)}{8 C_L L_m f^2} \qquad (46)$$

Here $f = \frac{1}{T}$ is the switching frequency.

Finally, the equation of the capacitor at the low voltage side is given as

$$C_L = \frac{(1 - \delta)}{8 \left(\Delta V_L / V_L \right) L_m f^2} \qquad (47)$$

Design of the inductor value:

According to the BDC under buck operation, the meant currents of load resistor and inductor are the same
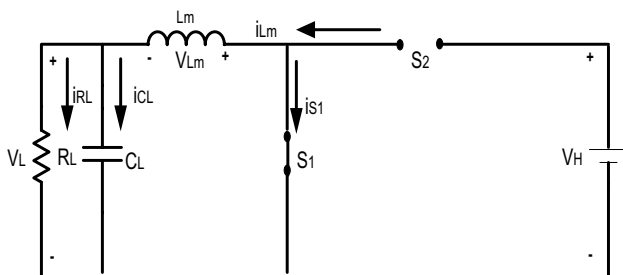
$$I_{Lm} = I_{RL} = \frac{V_L}{R_L} \qquad (48)$$

The maximum and minimum values of inductor currents can be expressed as

$$I_{Lm\_}\max = I_{Lm} + \frac{\Delta i_{Lm}}{2} = \frac{V_L}{R_L} + \frac{1}{2} \left[\frac{V_L}{L_m}(1 - \delta)T \right] = V_L \left[\frac{1}{R_L} + \frac{(1 - \delta)}{2 L_m f} \right] \qquad (49)$$

$$I_{Lm\_}\min = I_{Lm} - \frac{\Delta i_{Lm}}{2} = \frac{V_L}{R_L} - \frac{1}{2} \left[\frac{V_L}{L_m}(1 - \delta)T \right] = V_L \left[\frac{1}{R_L} - \frac{(1 - \delta)}{2 L_m f} \right] \qquad (50)$$

Under continuous current mode condition, the inductor current must be greater than zero

$$V_L \left[\frac{1}{R_L} - \frac{(1 - \delta)}{2 L_m f} \right] \geq 0 \qquad (51)$$

Therefore, the minimum inductance can be satisfied as

$$L_{m\_}\min \geq \frac{(1 - \delta) R_L}{2f} \qquad (52)$$

Further modifications the boost and buck mode of BDC inductance can be maintained for a continuous mode of operation

$$L_{m\_boost} = \frac{\delta(1 - \delta)^2 V_H^2}{2 P_H f} \qquad (53)$$

$$L_{m\_buck} = \frac{(1 - \delta) V_L^2}{2 P_L f} \qquad (54)$$

Here $P_H = \frac{V_H^2}{R_H}$ is the power at high voltage side, $P_L = \frac{V_L^2}{R_L}$ is the power at low voltage side.

Under any duty cycle for generating required voltage levels is given as

$$\frac{\delta(1 - \delta)^2 V_H^2}{2 P_H f} \geq \frac{(1 - \delta) V_L^2}{2 P_L f} \qquad (55)$$

5 Implementation of control strategy with MFB controller

The generation of pulse signal to the switches present in the converter can be represented in four different cases with flow chart representation in Figs. 13 and 14. Figure 13 representing that how the controlled pulse signals are generating and how they are giving to the switch corresponding to the speed of the drive especially in first two cases like heavy and more than rated load cases. Similarly, Fig. 14 representing the further two cases 3 and case 4 flowchart representation.

Figure 15 representing how the regulated pulse signals are generating to the switch three by the combination of
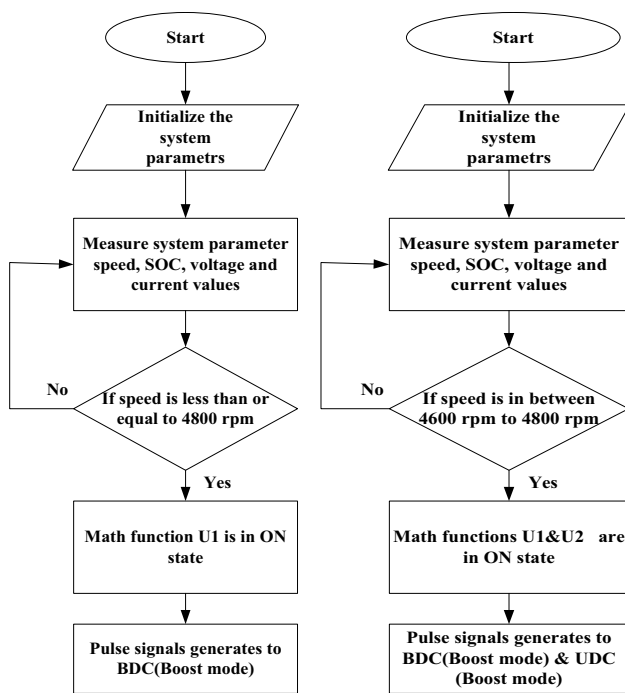

Fig. 12 DC–DC bidirectional converter representation under buck mode, switch S1 ON condition

Fig. 13 Flow chart representation during case-1 and 2 operation
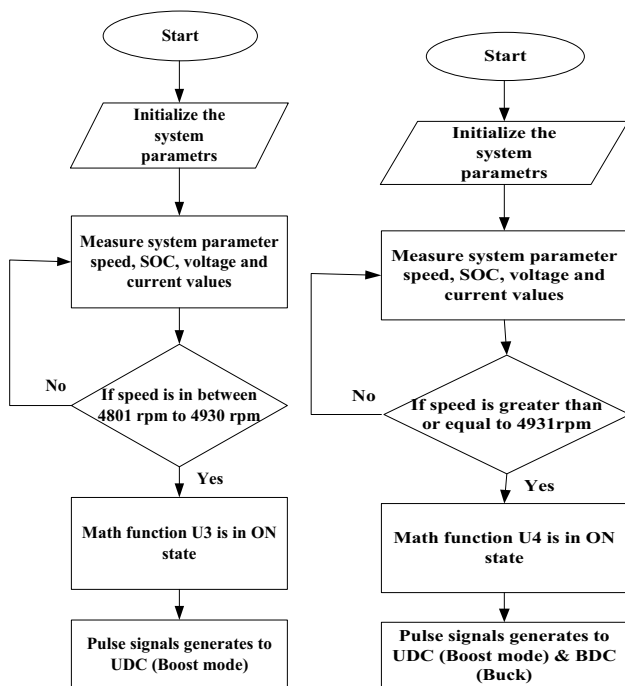

Fig. 14 Flow chart representation during case-3 and 4 operation

two-controller in that first one is MFB and the second one is the conventional controller. Figure 16 representing that the regulating pulse produced to switch one and three by the proposed hybrid controller. In the same way, Fig. 17 representing the regulating pulses are produced to switch

one by the hybrid controller action. Lastly, Fig. 18 is corresponding to the regulated pulses are given to the switch one and two by the designed hybrid controller action.

All regulated signals are produced to the switches because of the two controllers, in that conventional controllers always produces the controlled pulse signals, which can again regulate by the MFB controller corresponding to the speed of an electric motor.

Here MFB controller works with the speed of the motor which always depends upon the load applied. If the speed of the motor is less than or equal to 4800 rpm then MFB develops out the signal as one for U1. The speed of the motor is between 4600 and 4800 rpm then MFB develops output signals as one for U1 and U2. In the same way, the speed of the motor is between 4801 and 4930 rpm then MFB will develop the output signal as one for U3. Finally, if the speed value is greater than or equal to 4931 rpm then MFB develops output signal as one for U4. In this way, the MFB controller will develop the signals with speed as input which useful to regulate the pulse signals developed by the conventional controller.

Consider U1, U2, U3, and U4 as an output of the MFB controller, which can be represented with below equations and based on this relation the controlled signals are produced by the implemented control method.

$$U_1, U_2, U_3, U_4 = f(x)$$

$$f(x) = \begin{cases} U_1; x \leq 4800 \text{ rpm} \\ U_1 \&\& U_2; 4600 \text{ rpm} \leq x \leq 4800 \text{ rpm} \\ U_3; 4801 \text{ rpm} \leq x \leq 4930 \text{ rpm} \\ U_4; x \geq 4931 \text{ rpm} \end{cases}$$

6 Output results and discussion

In this section, the MATLAB/Simulink results are presented and discussed related four different cases. Mainly all results are obtained with two different hybrid controllers named as MFB with ANN and MFB with PID. And in this section speed, current and regulated pulse signals waveforms are plotted to correspond to each controller case. The first case is related to a heavy load, the second one is corresponding to more than rated load, in case three rated load is applied and finally in the fourth case motor is running with no load.

6.1 Case-1 output results

Figure 19 shows that the comparison of two hybrid controllers speed waveform during case-1 corresponding to the load applied. From those two controllers MFB with ANN has reached the stable state 0.75 s, on the other hand,

Fig. 15 controlled pulse signals generation to only BDC under boost operation
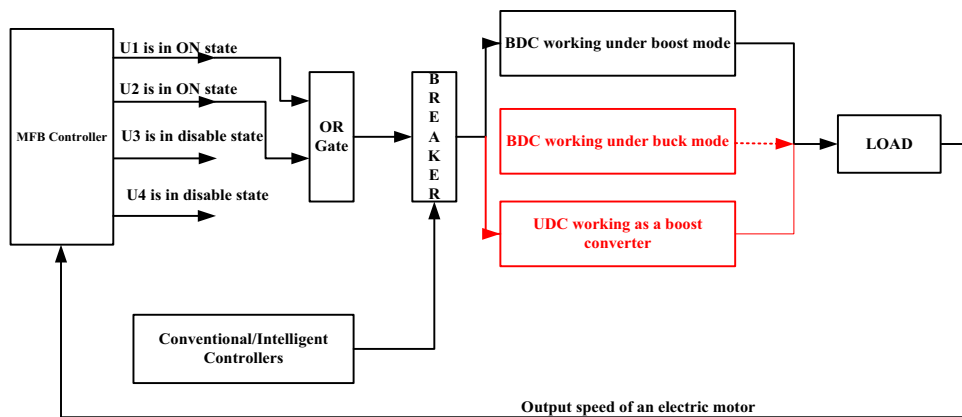

Fig. 16 controlled pulse signals generation to UDC and BDC under boost operation
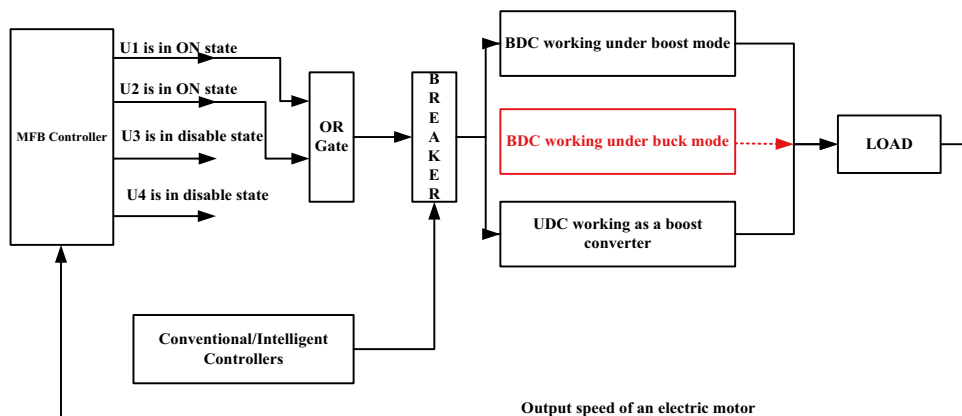

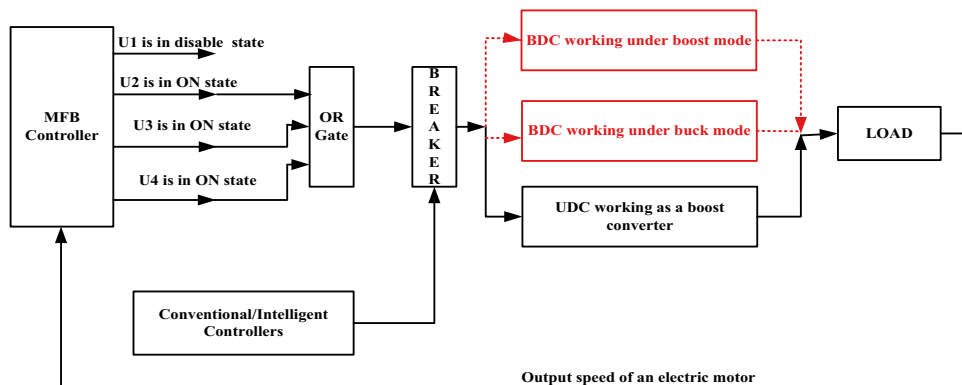**Fig. 17** controlled pulse signals generation to only UDC under boost operation

Fig. 18 controlled pulse signals generation to UDC as boost and BDC under buck operation
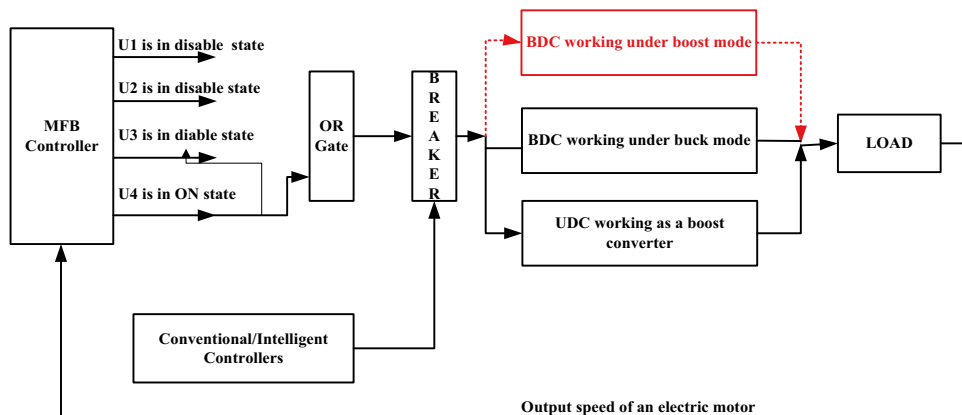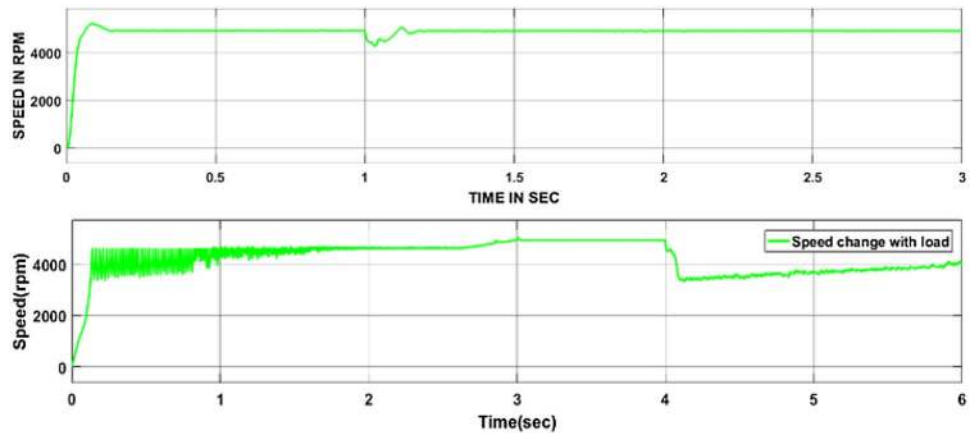
Fig. 19 Output responses of the motor during a heavy load condition by MFB with ANN MFB with PID controllers

MFB with PID controller response not attained the stable state.

Figure 20 shows the regulated signals produced by the MFB with ANN to the converters corresponding to the case-1.

Figure 21 shows the regulated signals produced by the MFB with PID to the converters corresponding to the case-1.

6.2 Case-2 output results

Figure 22 shows that the comparison of two hybrid controllers speed waveforms during case-2 corresponding to the load applied. From those two controllers MFB with ANN has reached the stable state 0.25 s, on the other hand, MFB with PID took 0.5 s.

Figure 23 shows the regulated signals produced by the MFB with ANN to the converters corresponding to the case-2.

Figure 24 shows the regulated signals produced by the MFB with PID to the converters corresponding to the case-2.

6.3 Case-3 output results

Figure 25 shows that the comparison of two hybrid controllers speed waveform during case-3 corresponding to the load applied. From those two controllers, MFB with ANN has reached a stable state 0.1 s, on the other hand, MFB with PID took 0.15 s.

Figure 26 shows the regulated signals produced by the MFB with ANN to the converters corresponding to the case-3.
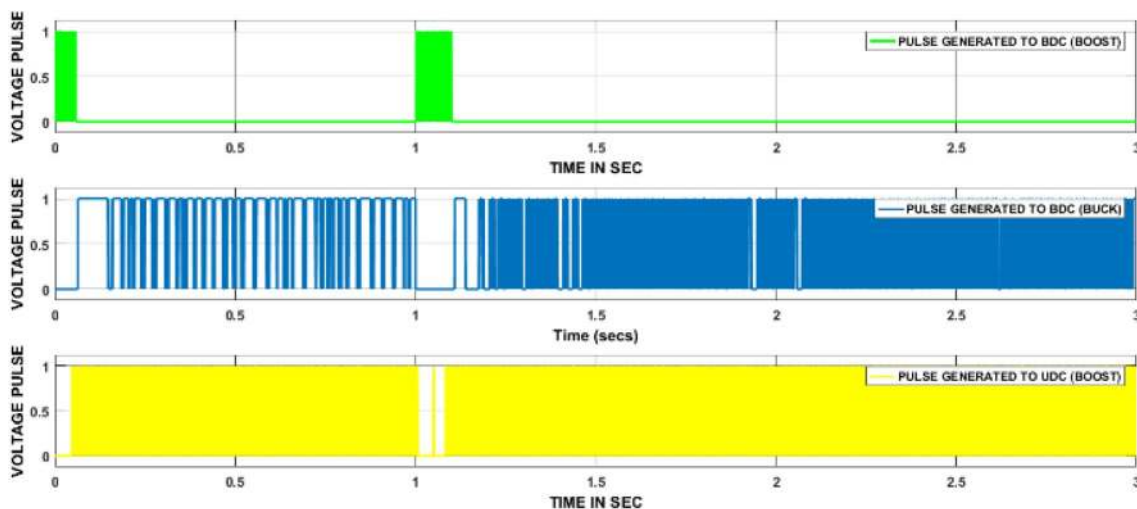
Fig. 20 Controlled switching signals produced by the MFB with ANN controller to BDC as well as UDC
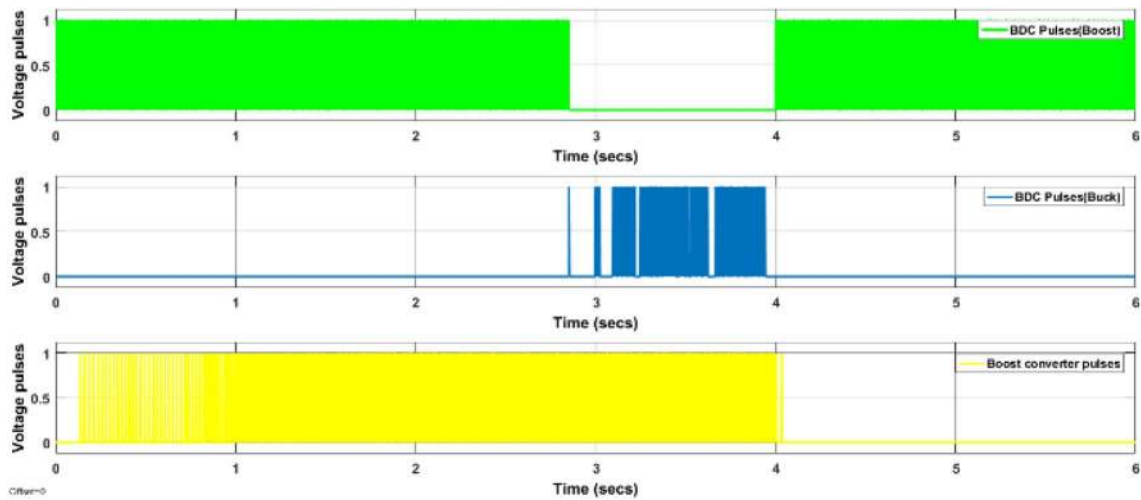
Fig. 21 Controlled switching signals produced by the MFB with PID controller to BDC as well as UDC

Fig. 22 Output responses of the motor during slightly more than rated load condition by MFB with ANN, MFB with PID controllers
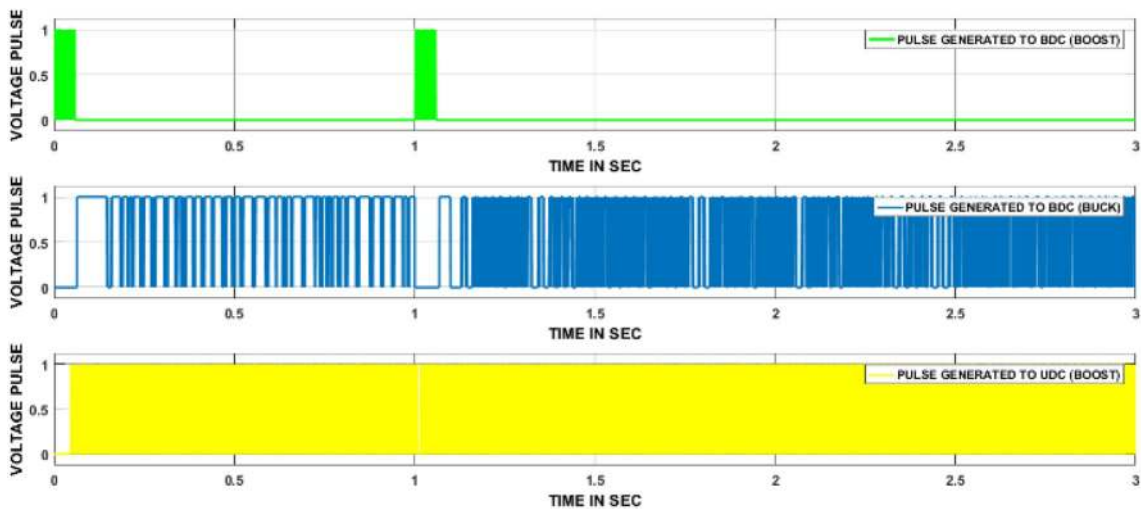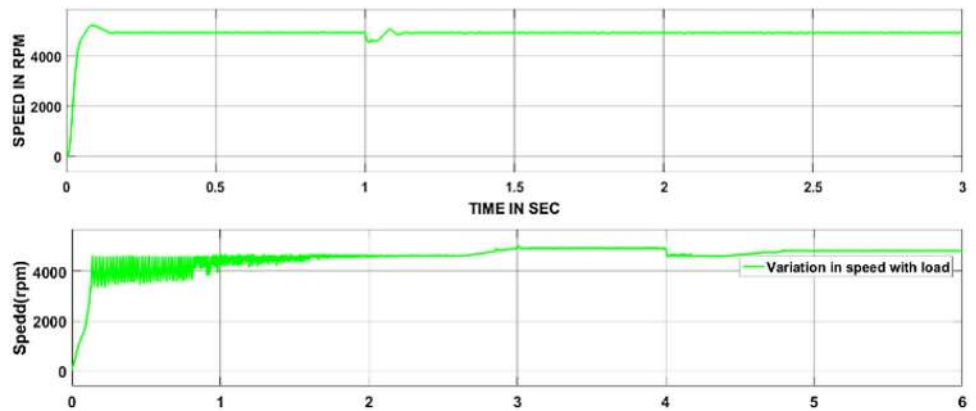

Fig. 23 Controlled switching signals produced by the MFB with ANN controller to BDC as well as UDC

Fig. 24 Controlled switching signals produced by the MFB with PID controller to BDC as well as UDC

Fig. 25 Output responses of the motor during a rated load condition by MFB with ANN, MFB with PID controllers

Fig. 26 Controlled switching signals produced by the MFB with ANN controller to BDC as well as UDC
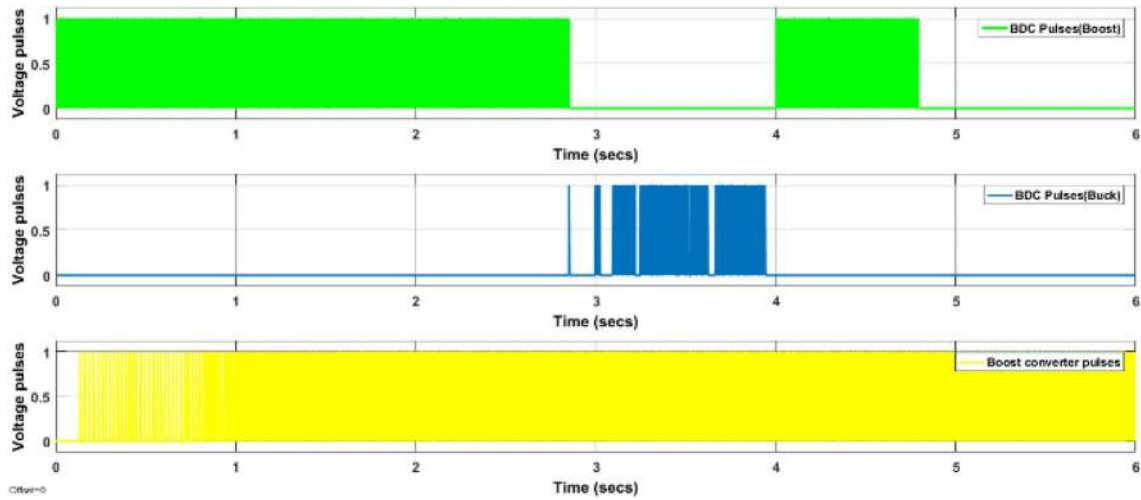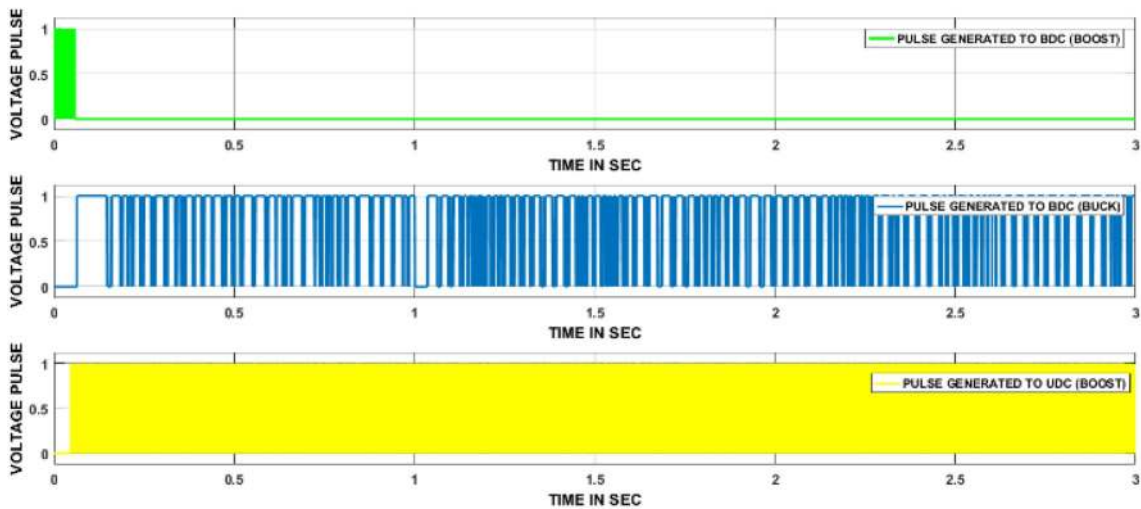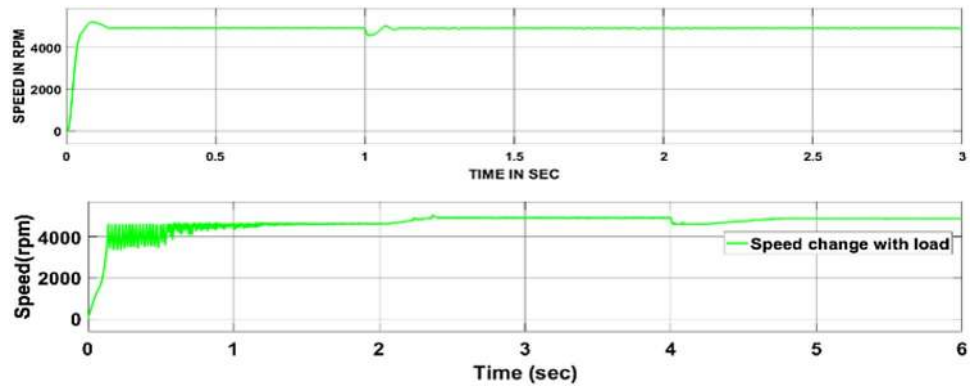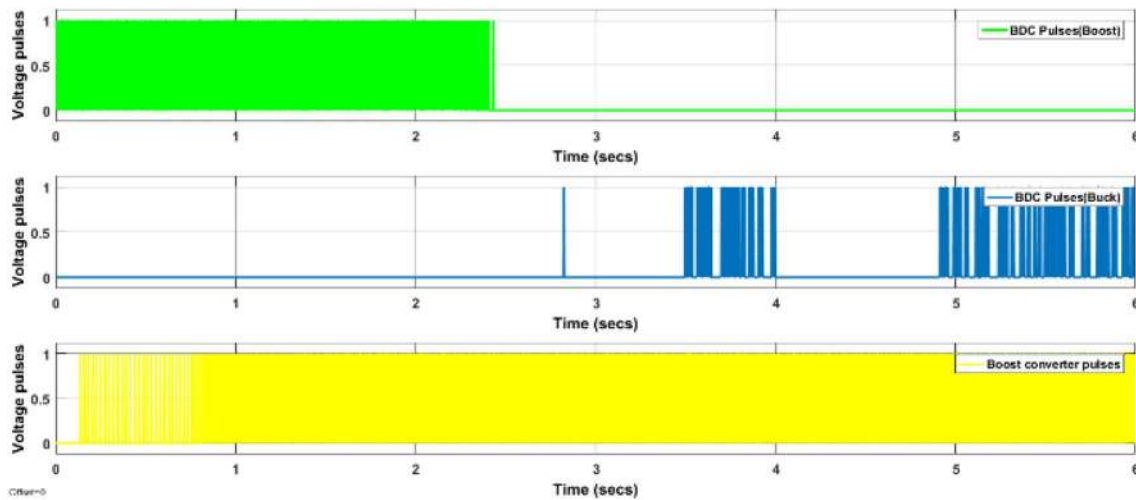
Fig. 27 Controlled switching signals produced by the MFB with PID controller to BDC as well as UDC

Fig. 28 Output responses of the motor during a no-load condition by MFB with ANN, MFB with PID controllers
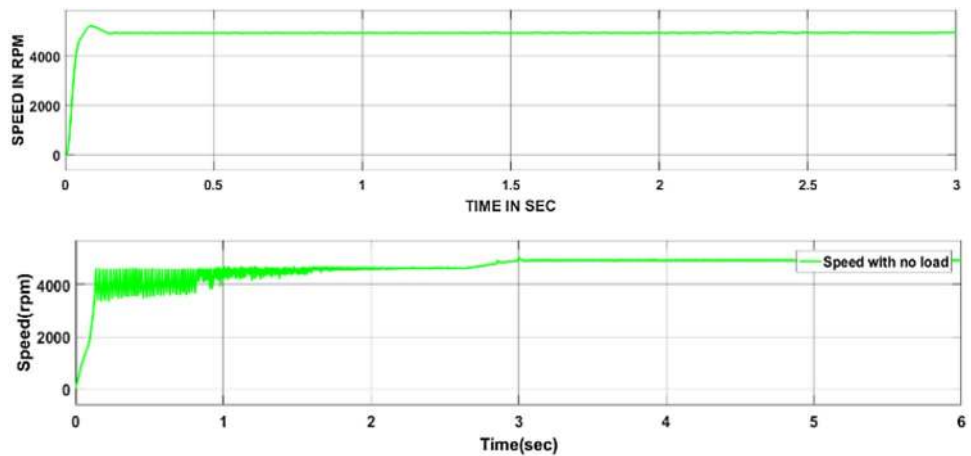

6.4 Case-4 output results

Figure 28 shows that the comparison of two hybrid controllers speed waveform during case-4 corresponding to the no-load applied.

Figure 29 shows the regulated signals produced by the MFB with ANN to the converters corresponding to the case-4.

Figure 30 shows the regulated signals produced by the MFB with PID to the converters corresponding to the case-4.

6.5 Converters output waveforms

Figure 31 is representing the output parameters of the BDC, and which clearly saying that the negative current indicates UC charging, on the other hand, positive current indicates the discharge time of the UC.

Figure 32 shows that the output parameters of UDC and both current and voltage are maintained constantly corresponding to the applied load.

Table 1 is representing the two-hybrid controllers' performances in four cases in terms of their settling time after applying different loads. In case one MFFB with ANN has taken 0.75 s to steady-state whereas MFB with PID response has not reached the steady-state within the stipulated time. During case two, both controllers are reached the steady-state with 0.25 s and 0.5 s time. In case three also two controllers are taken different timing 0.1 s, 0.15 s to reach steady state. In the fourth case no load is applied
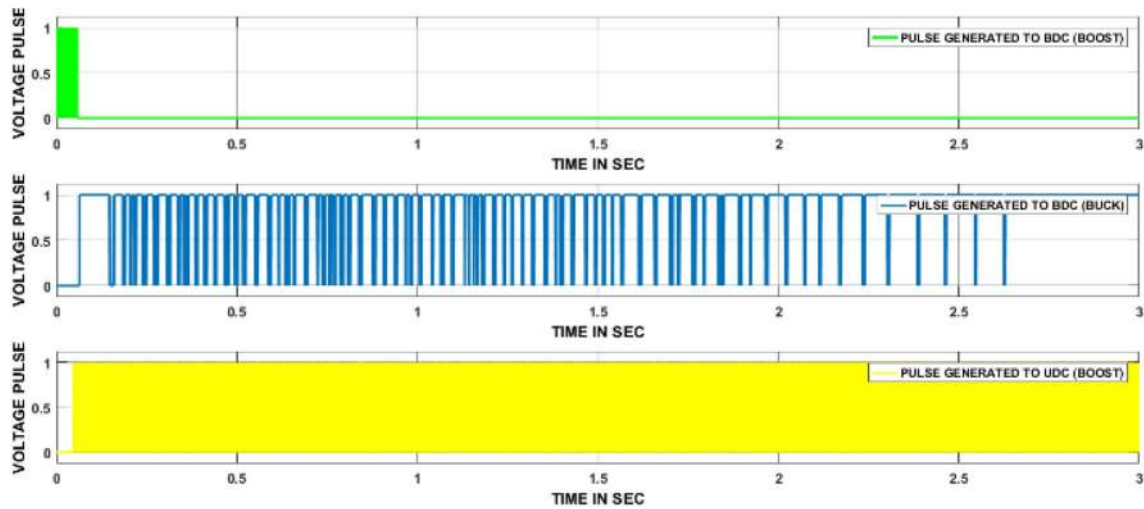
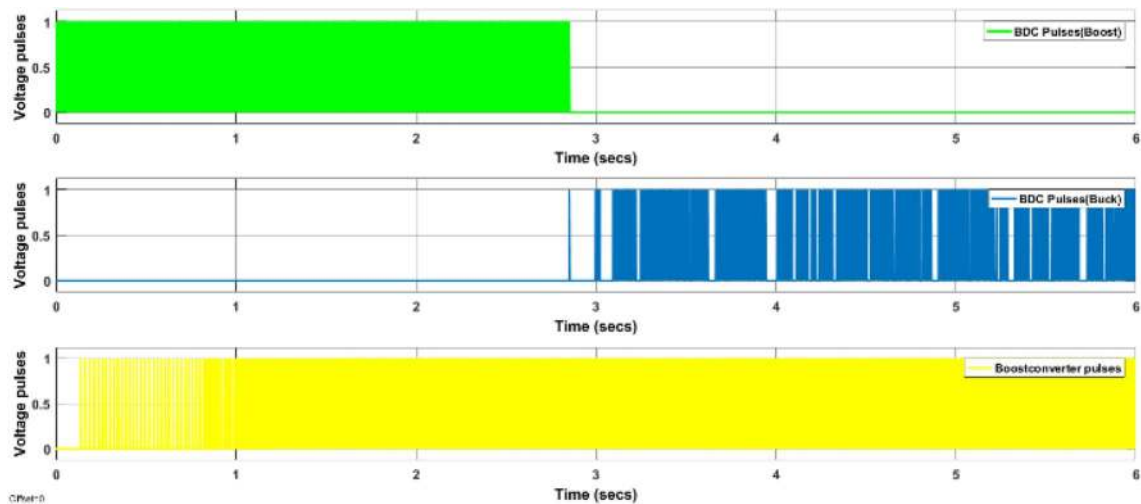**Fig. 29** Controlled switching signals produced by the MFB with ANN controller to BDC as well as UDC

Fig. 30 Controlled switching signals produced by the MFB with PID controller to BDC as well as UDC

to the motor, so controller action not required in this case to reach steady but requires developing the regulated pulse to the switches of converters.

7 Conclusion

Table 2 is representing the comparisons between two hybrid controllers based on the time domain specifications. Here MFB with ANN has provided better performance than the MFB with PID in all aspects except maximum peak overshoot.

Table 3 shows that the performance comparisons between two controllers particularly during starting and

rated load condition by taking steady-state time as a reference. In this study, the MFB with ANN given better performance by taking less time period to reach stable state.

The hybrid controller is designed by combining MFB controller with conventional/intelligent controller, based on the proposed control strategy approach two different hybrid controllers MFB with ANN, MFB with PID are designed and obtained the satisfactory results from both controllers in four modes of operation. Among all the controllers MFB played a vital role during switching of energy sources from one to another based on the speed of an electric motor. Two-hybrid controller's performance study is made with different time domain specifications and all are tabulated in the conclusion section.
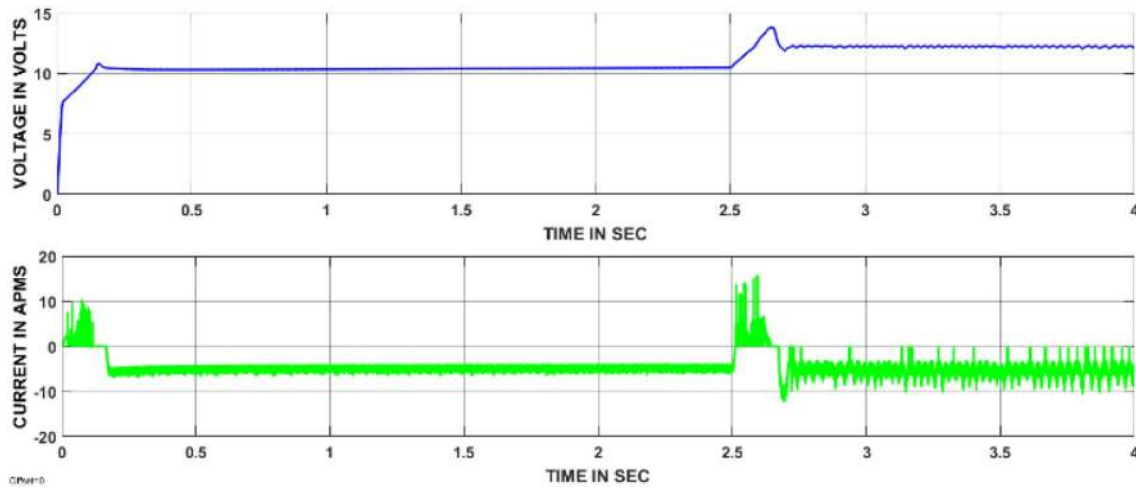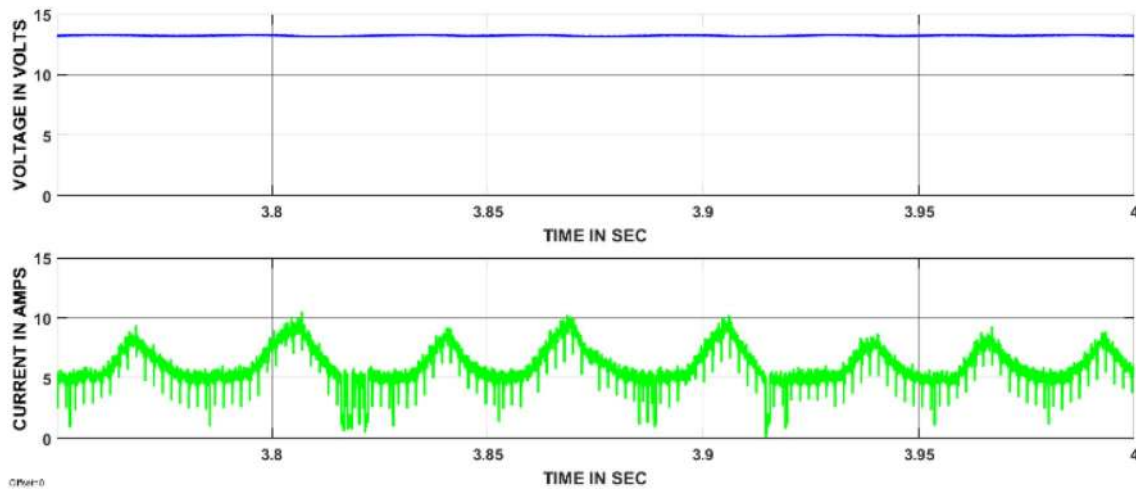
Fig. 31 Output parameters of BDC

Fig. 32 Output parameters of UDC

Table 1 Performance analysis between two controllers after applying load on the electric motor

Controller type	The steady-state time corresponding to different loads (s)			
	Case-I	Case-II	Case-III	Case-IV
MFB with ANN	0.75	0.25	0.1	No load applied
MFB with PID	Not settled	0.5	0.15	No load applied

Table 2 Performance analysis of controllers based on time-domain specifications

Controller type	Delay time (s)	Rise time (s)	Peak time (s)	Settling time (s)	Maximum peak overshoot (%)
MFB with ANN	0.05	0.08	0.1	0.6	12
MFB with PID	0.25	1.6	1.7	1.8	4.16

Table 3 Performance analysis between controllers with and without load condition

Controller type	Steady-state time at starting (s)	Steady-state time at rated load (s)
MFB with ANN	0.15	0.1
MFB with PID	1.6	0.15

Compliance with ethical standards

Conflict of interest The authors declare that they have no conflict of interest.

Appendix 1

See Table 4.

Table 4 Internal parameter of UC

Rated capacitance (F)	5
DC series resistance (Ω)	2.1e−3
Rated voltage (V)	6

Appendix 2

See Table 5.

Table 5 Battery parameters

Nominal voltage (V)	6
Rated capacity (Ah)	3.6
Initial state-of-charge (%)	99
Battery response time (s)	10

Appendix 3

See Table 6.

Table 6 Motor parameters

Rated voltage (V)	12
Power (HP)	0.268
Speed (RPM)	5000
Stator phase resistance Rs (Ω)	1.16/2

Appendix 4

See Table 7.

Table 7 Converter parameters

Inductance (H)	300e−3
Capacitance (F)	220e−6
Resistance(Ω)	0.1

References

1. Shen J, Khaligh A (2016) Design and real-time controller implementation for a battery-ultracapacitor hybrid energy storage system. IEEE Trans Ind Inform 12(5):1910–1918
2. Camara MB, Gualous H, Gustin F, Berthon A (2008) Design and new control of DC/DC converters to share energy between supercapacitors and batteries in hybrid vehicles. IEEE Trans Veh Technol 57(5):2721–2735
3. Francoise JNM, Gualous H, Outbib R, Berthon A (2005) 42 V power net with supercapacitor and battery for automotive applications. J Power Sources 143(1/2):275–283
4. Trovao JPF, Santos VD, Antunes CH, Pereirinha PG, Jorge HM (2015) A real-time energy management architecture for multi-source electric vehicles. IEEE Trans Ind Electron 62(5):3223–3233
5. Cho HY, Gao W, Ginn HL (2004) A new power control strategy for hybrid fuel cell vehicles. In: Proceedings of IEEE power electronic transportation, Oct 21–22, pp 159–166
6. Dusmez S, Khaligh A (2014) A supervisory power-splitting approach for a new ultracapacitor–battery vehicle deploying two propulsion machines. IEEE Trans Ind Inform 10(3):1960–1971
7. Wang B, Xu J, Cao BG, Zhou X (2015) A novel multimode hybrid energy storage system and its energy management strategy for electric vehicles. J Power Sources 281:432–443
8. Palma L, Enjeti P, Howze JW (2003) An approach to improve battery run-time in mobile applications with supercapacitors. In: Proceedings of IEEE Power Electronics Conference, June 15–19, vol 2, pp 918–923
9. Atmaja TD (2015) Energy storage system using battery and ultracapacitor on a mobile charging station for an electric vehicle. Energy Procedia 68:429–437
10. Lhomme W, Delarue P, Barrade P, Bouscayrol A, Rufer A (2005) Design and control of a supercapacitor storage system for traction applications. In: Conference record IEEE IAS annual meeting, Oct 2–6, vol 3, pp 2013–2020
11. Hart DW (2003) Introduction to power electronics. Prentice-Hall, New York